The official journal of
INTERNATIONAL FEDERATION OF PIGMENT CELL SOCIETIES · SOCIETY FOR MELANOMA RESEARCH

PIGMENT CELL & MELANOMA Research

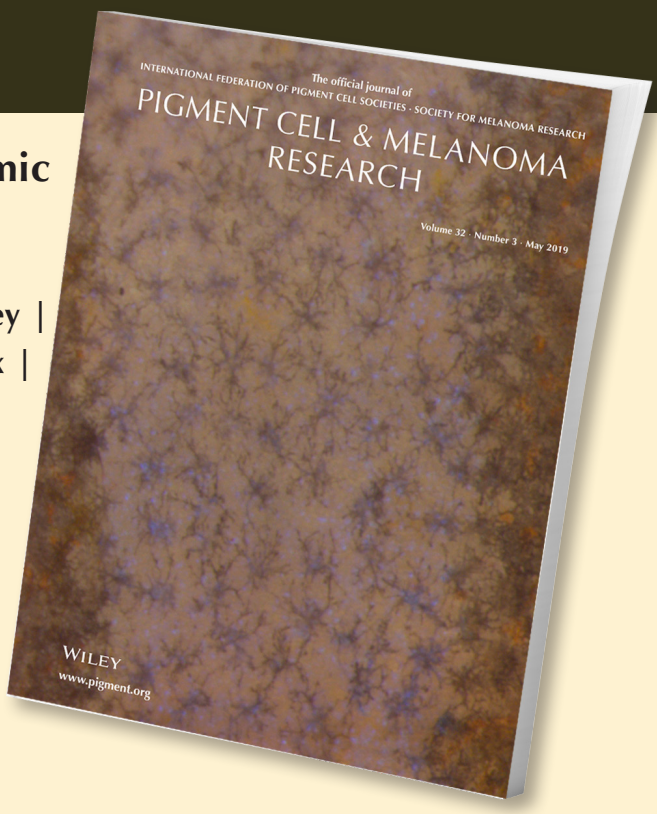

Developmental and comparative transcriptomic identification of iridophore contribution to white barring in clownfish

Pauline Salis | Thibault Lorin | Victor Lewis | Carine Rey | Anna Marcionetti | Marie-Line Escande | Natacha Roux | Laurence Besseau | Nicolas Salamin | Marie Sémon | David Parichy | Jean-Nicolas Volff | Vincent Laudet

DOI: 10.1111/pcmr.12766

Volume 32, Issue 3, Pages 391–402

Received: 29 August 2018 | Revised: 11 December 2018 | Accepted: 26 December 2018

DOI: 10.1111/pcmr.12766

ORIGINAL ARTICLE

WILEY

Developmental and comparative transcriptomic identification of iridophore contribution to white barring in clownfish

Pauline Salis[1*] | Thibault Lorin[2*] | Victor Lewis[3,4] | Carine Rey[5,6] | Anna Marcionetti[7,8] | Marie-Line Escande[1] | Natacha Roux[1] | Laurence Besseau[1] | Nicolas Salamin[7,8] | Marie Sémon[5] | David Parichy[4] | Jean-Nicolas Volff[2] | Vincent Laudet[1]

[1]Observatoire Océanologique de Banyuls-sur-Mer, UMR CNRS 7232 BIOM, Sorbonne Université, Banyuls-sur-Mer, France

[2]IGFL, ENS de Lyon, UMR 5242 CNRS, Université Claude Bernard Lyon I, Lyon Cedex 07, France

[3]Department of Biology, University of Washington, Seattle, Washington

[4]Department of Biology, Department of Cell Biology, University of Virginia, Charlottesville, Virginia

[5]ENS de Lyon, CNRS UMR 5239, INSERM U1210, LBMC, Université Claude Bernard, Lyon, France

[6]LBBE, CNRS, Université Lyon 1, Villeurbanne, France

[7]Department of Computational Biology, Biophore, University of Lausanne, Lausanne, Switzerland

[8]Swiss Institute of Bioinformatics, Lausanne, Switzerland

Correspondence
Vincent Laudet, Observatoire Océanologique de Banyuls-sur-Mer, Banyuls-sur-Mer, France.
Email: vincent.Laudet@obs-banyuls.fr

Funding information
CNRS Interdisciplinarity Actions; EMBRC-France, Grant/Award Number: ANR-10-INBS-02; NIH, Grant/Award Number: R35 GM122471

Abstract

Actinopterygian fishes harbor at least eight distinct pigment cell types, leading to a fascinating diversity of colors. Among this diversity, the cellular origin of the white color appears to be linked to several pigment cell types such as iridophores or leucophores. We used the clownfish *Amphiprion ocellaris*, which has a color pattern consisting of white bars over a darker body, to characterize the pigment cells that underlie the white hue. We observe by electron microscopy that cells in white bars are similar to iridophores. In addition, the transcriptomic signature of clownfish white bars exhibits similarities with that of zebrafish iridophores. We further show by pharmacological treatments that these cells are necessary for the white color. Among the top differentially expressed genes in white skin, we identified several genes (*fhl2a*, *fhl2b*, *saiyan*, *gpnmb*, and *apoD1a*) and show that three of them are expressed in iridophores. Finally, we show by CRISPR/Cas9 mutagenesis that these genes are critical for iridophore development in zebrafish. Our analyses provide clues to the genomic underpinning of color diversity and allow identification of new iridophore genes in fish.

KEYWORDS
Amphiprion, clownfish, coral reef fish, iridophore, leucophore, transcriptomic

1 | INTRODUCTION

Patterns of adult pigmentation provide an outstanding opportunity to define the interplay between ecology, development, and genetics that is the basis for trait diversification (Cuthill et al., 2017). Some of the most compelling pigmentation features in vertebrates occur in actinopterygian fishes, which include more than 30,000 species displaying a wide variety of color patterns and pigment cells (Lorin, Brunet, Laudet, & Volff, 2018). Indeed, while mammals only have one pigment cell type, the melanocyte, actinopterygians harbor at least eight types of pigment cells: melanophores, iridophores, and xanthophores but also erythrophores, leucophores, cyanophores, erythro-iridophores, cyano-erythrophores, and even fluorescent cells (Fujii, 1993; Schartl et al., 2015). Consequently, in the last

*These author contributed equally to this work.

decades, the field of vertebrate pigmentation has much benefited from the introduction of actinopterygian model species, such as zebrafish, medaka, or cichlid fishes (Santos et al., 2014).

Studies of laboratory model teleosts have contributed to the current understanding of genetic and cellular mechanisms underlying pigment development and patterning (Frohnhöfer, Krauss, Maischein, & Nüsslein-Volhard, 2013; Hirata, Nakamura, Kanemaru, Shibata, & Kondo, 2003; Nakamasu, Takahashi, Kanbe, & Kondo, 2009; Patterson & Parichy, 2013; Watanabe & Kondo, 2015). For example, zebrafish *Danio rerio* harbors three major classes of pigment cells—carotenoid- and pteridine-containing xanthophores that provide the yellow/orange hue; reflective purine-containing iridophores, and melanin-containing black melanophores—that are themselves divided into genetically and developmentally distinct subclasses (Eom, Bain, Patterson, Grout, & Parichy, 2015; Hirata et al., 2003; McMenamin et al., 2014). These pigment cells interact with each other and other cell types to provide the characteristic dark stripes and light interstripes of *D. rerio* (Eom & Parichy, 2017; Singh & Nusslein-Volhard, 2015). Likewise, medaka *Oryzias latipes* has been employed to understand the mechanisms that specify pigment cell fates, including those required by yellow–white leucophores, which are ultrastructurally and genetically distinct from iridophores (Kimura et al., 2014; Kimura, Takehana, & Naruse, 2017; Nagao et al., 2014; Nagao et al., 2018).

Among actinopterygians, coral reef fish exhibit an extraordinary set of colors and patterns, therefore providing ample material to study the cellular and genomic basis of color diversity in vertebrates. Here, we used the clownfish *Amphiprion ocellaris*, which exhibits an adult color pattern of distinctive, vertical white bars over a dark orange body (Salis et al., 2018). White bars exhibit a matte coloration that is qualitatively different from the iridescent light interstripes of zebrafish, and the cellular bases and genetic requirements of white barring have not been characterized. Here, we asked whether the white bars of *A. ocellaris* are composed of iridophores, as in zebrafish interstripes, whitish leucophores similar to those present scattered in medaka, or both types of cell. Using electron microscopy and transcriptomic analysis, we find that white cells of *A. ocellaris* resemble iridophores. We further show that several genes expressed specifically in white bars are required for iridophore development in zebrafish, including loci not previously identified for having such roles. Finally, using pharmacological manipulations, we show that *A. ocellaris* iridophores and zebrafish iridophores share a common dependence on anaplastic lymphoma kinase and leukocyte tyrosine kinase (ALK/LTK) signaling. Taken together, our results indicate that the white bars of clownfish comprise densely packed iridophores, illustrating the diverse pattern elements that can be generated by a conserved set of pigment cell classes.

Significance

Coral reef fish exhibit an extraordinary set of colors and patterns, therefore providing ample material to study the cellular and genomic basis of color diversity in vertebrates. Here, we asked whether *Amphiprion ocellaris* clownfish's white bars depend on iridophores, as in zebrafish interstripes, or on leucophores, as found in medaka. Using electron microscopy, transcriptomic analysis, and genetic approaches, we reveal that white cells of *A. ocellaris* are iridophores. Our data illustrate the diverse pattern elements that can be generated by a conserved set of pigment cell classes.

2 | MATERIALS AND METHODS

2.1 | Stereomicroscope image processing

White and orange skins were imaged using Zeiss stereomicroscope (V20 discovery-Plan S objective 1.0×) using a VisiLED Brightfield Ringlight S80 for incident lighting. All the images were taken using a full homogenized lighting. However, iridescent cells of the white skin were only visible when using segmental lighting. Images were processed using a camera (Axiocam 105) with a picture resolution of 1280X960 pixels. Pictures of high magnification of skin (Figure 1 and Supporting Information Figures S1) were done using 30 ms of time exposure. Pictures of full individuals (Figure 2) were done always in the same lighting conditions with an exposure time of 10 ms. White balance was set up at the beginning of each experiment to get the same image properties. A post-process was done on original images to increase contrast using IMAGEJ software.

2.2 | Transmission electron microscopy

Amphiprion ocellaris 3–4 cm individuals were euthanized using 200 mg/L of MS-222 Tricaine-S. White and orange skins were dissected in a mixture of 3% paraformaldehyde/3% glutaraldehyde in 0.1 M cacodylate buffer (pH 7.2), and fixed overnight at 4°C, according to Djurdjevič, Kreft, and Sušnik Bajec (2015). After 1% OsO_4 post-fixation (1 hr at RT), individuals were dehydrated in a graded series of ethanol solutions and embedded in Epon 812 resin (Electron Microscopy Science). Ultra-thin (80 nm) sections were cut using a Leica Ultracut R microtome, contrasted with uranyl acetate and lead citrate, and examined with a Hitachi H7500 TEM.

2.3 | RNA extraction and purification for qPCR and transcriptomic skin experiments

Amphiprion ocellaris and *Amphiprion frenatus* adults (3–4 cm) were euthanized prior to dissection in MS222 at 200 mg/L (three individuals per experiment). A shallow incision was made with a razor in the white body bar and orange skin (posterior to the white body bar) regions from both sides of the body fish *A. ocellaris* (Supporting Information Figure S2) and in the head white bar and orange body skin regions of the body fish *A. frenatus*. The skin was slowly pulled back with forceps while using the razor blade to make sure the skin separated cleanly from the underlying tissue and conserved

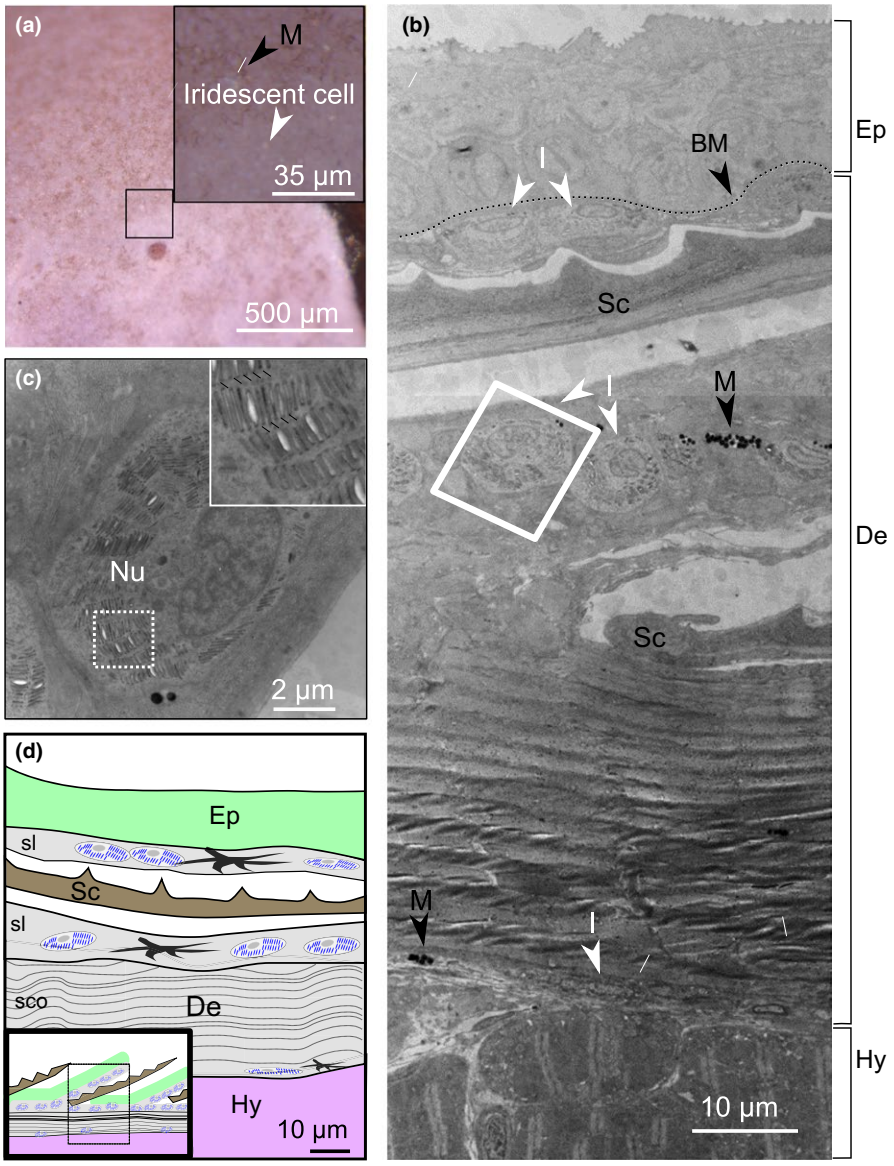

FIGURE 1 Pigment cell organization in white skin of *Amphiprion ocellaris*. (a) Stereomicroscope image of white skin in a living *A. ocellaris* juvenile showing iridescent cells (white arrowhead) and melanophores (black arrowhead). Image shown is typical of 20 individuals inspected. (b, c) Transmission electron microscopy (TEM) image of a transverse section through white bar skin. The various skin layers are indicated. (c) High magnification of an iridophore (boxed in c) showing parallel platelets (inset). (d) Cartoon representing a transverse section of the white skin of *A. ocellaris* with iridophores (represented by the blue round cells) and melanophores (black star cells). The majority of pigment cells are found in the stratum laxum of the dermis (gray). (BM: basal membrane; De: dermis; Ep: epidermis; Hy: hypodermis; I: iridophores; M: melanophores; Nu: nucleus, Sc: scale; sco: stratum compactum; sl: stratum laxum). All TEM experiments have been replicated in four individuals [Colour figure can be viewed at wileyonlinelibrary.com]

in RNAlater until RNA extraction. The RNA was extracted using TRIzol (TRIzol Reagent 15596-026 Kit; Ambion) followed by DNase treatment (DNA-free AM1906 Kit; Ambion) and then purified with 0.025 µm dialysis membranes to remove reverse transcriptase inhibitors.

2.4 | RNA-Seq library preparation and sequencing

RNA-Seq libraries were generated with TruSeq Stranded mRNA Sample Preparation Kit (Illumina) from 400 ng of total RNA using skin samples according to manufacturer's instructions. Surplus PCR primers were removed using AMPure XP beads (Beckman Coulter). Final cDNA libraries were checked for quality and quantified using capillary electrophoresis. Libraries were loaded in the flow cell at 2 nM. Clusters were generated in the Cbot and sequenced on an Illumina HiSeq 4000 as single-end 50 base reads or paired-end 100 base reads.

2.5 | Reference transcriptome assembly and annotation

Adapter dimer reads of skin paired-end data were removed in silico using DimerRemover (https://sourceforge.net/projects/dimerremover/). Adapter trimming was conducted using BBDuk (https://sourceforge.net/projects/bbmap/; Supporting Information Figure S2). Reads corresponding to rRNAs were removed using SORTMERNA v2.1 (Kopylova, Noé, & Touzet, 2012) with *Oreochromis niloticus* rRNAs downloaded from ENSEMBL BIOMART v88 as reference. Reads were normalized using the *insilico_read_normalization.pl* tool in TRINITY v2.3.2 (Grabherr et al., 2011).

To obtain a genome-guided transcriptome assembly, reads were mapped to the *A. ocellaris* genome using HISAT2 v2.0.5 (Kim, Langmead, & Salzberg, 2015). Mapping results were further processed using SAMTOOLS v1.3.1 (Li et al., 2009). Assembly was performed using Trinity with default parameters (Grabherr et al.,

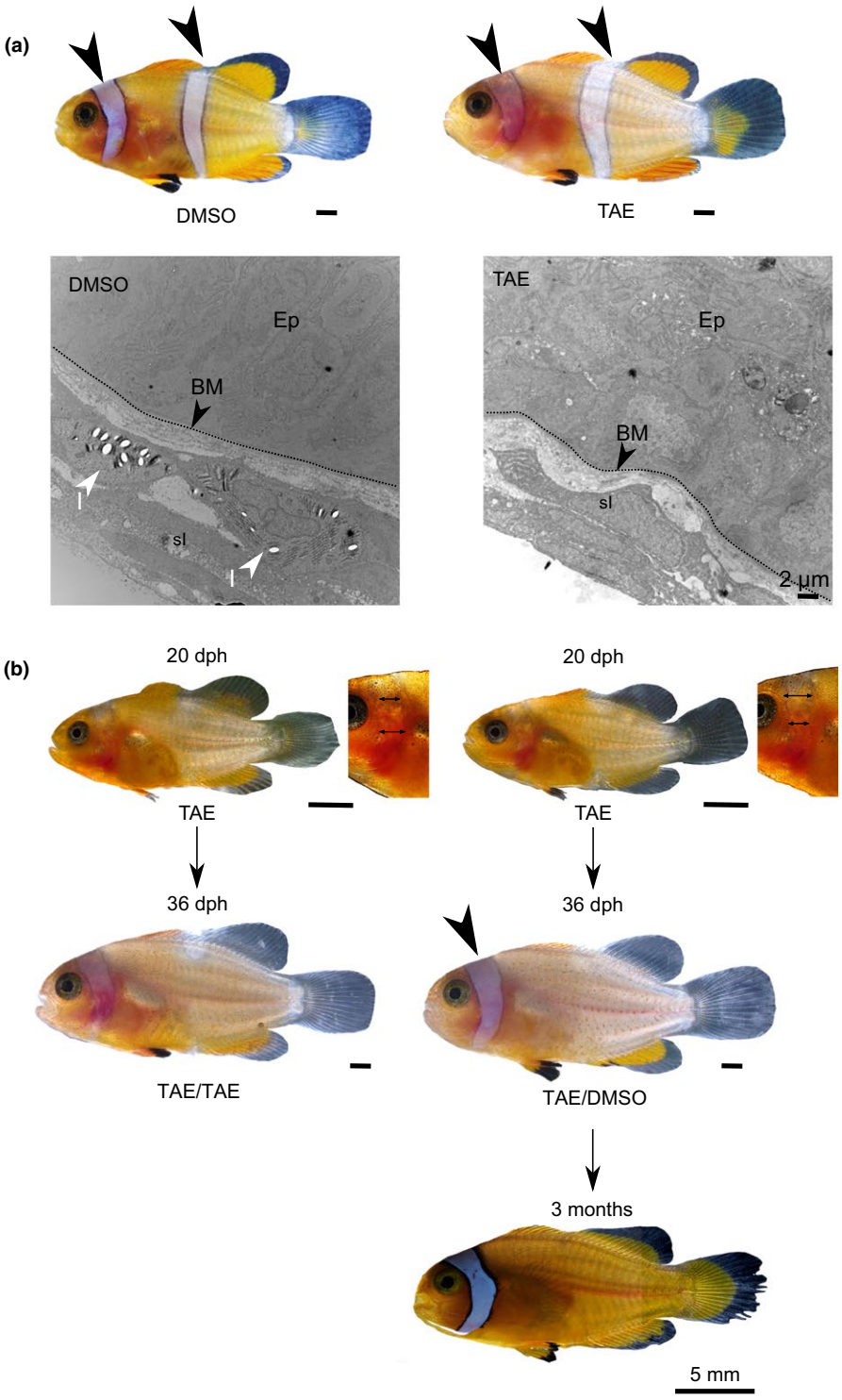

FIGURE 2 Iridophore survival control the white hue. (a—upper photographs) Effect of TAE 684 on white bars in juveniles. Stereomicroscope picture of clownfish juveniles of 36 days old treated from 20 dph until 36 dph with DMSO (left) or 0.6 µM TAE 684 (right). (a—bottom photographs) TEM images of transverse sections through the white body bar of clownfish juveniles (3 months dph) treated during 16 days with DMSO (left) or 0.6 µM TAE 684 (right). (b) Effect of removal of TAE 684 on white bars in juvenile. Left: Pictures of a clownfish individual treated with TAE 0.6 µM from 5 dph until 20 dph (20 dph—up) and kept in the drug for 16 days more (36 dph—bottom). Right: Pictures of a clownfish individual treated with TAE 0.6 µM from 5 dph until 20 dph (20 dph—up) and then treated with DMSO only from 20 dph until 3 months (36 dph—middle; 3 months—bottom). (BM: basal membrane; Ep: epidermis; I: iridophores; sl: stratum laxum of dermis). TAE experiments have been replicated in 10 individuals [Colour figure can be viewed at wileyonlinelibrary.com]

2011). In addition to the genome-guided assembly, we obtained a de novo transcriptome assembly from the same set of reads and combined both assemblies before identification of coding regions using TRANSDECODER v3.0.1 (http://transdecoder.sf.net). We used information from the closely related species *Stegastes partitus* to annotate *A. ocellaris* contigs with best BLASTN hit (*-task blastn -word_size 11 –e 1e-5*).

2.6 | Quantification, differential expression, and gene set enrichment analyses

We used KALLISTO v0.43.0 to align reads originating from single-end skin samples to the reference transcriptome and to quantify transcript abundance. Estimated counts were imported in R using *tximport* package (Soneson, Love, & Robinson, 2015). Differential expression

(DE) analysis was performed using DESEQ2 v1.14.1 testing for color variations with the individual effect included in the design (Love, Huber, & Anders, 2014). Gene set enrichment analyses were performed with Java implementation of the GSEA software (http://software.broadinstitute.org/gsea/index.jsp; Subramanian et al., 2005).

2.7 | Phylogenetic analyses

To ensure the identity of the 10 most differentially expressed genes (DEGs) in each condition, we conducted phylogenetic analyses. Using *S. partitus* sequences as query, sequences corresponding to best BLASTN hits were retrieved in multiple vertebrate species using Ensembl. Alignment was performed using Clustal Omega implemented in SEAVIEW v4.6.1 using default parameters. After manual curation, phylogenetic trees were built using maximum likelihood and the LG model of amino acid substitution as implemented in PHYML v3.1 within Seaview. Support for the most likely tree was based on the SH-aLRT algorithm (Anisimova, Gil, Dufayard, Dessimoz, & Gascuel, 2011). Phylogenetic trees and corresponding alignments are available at: http://igfl.ens-lyon.fr/equipes/j.-n.-volff-fish-evolutionary-genomics/lorin_additional_data/salis_lorin_pigmentation_skin_aocellaris/salis_lorin_supp-trees-top-degs.

2.8 | qRT-PCR assays

qRT-PCR primers were designed to anneal on different exons (see Supporting Information Table S1), and *rpl32* was used as a normalization gene. qRT-PCRs were performed in 96-well plate with KAPA SYBR Fast ABI ReadyMix Kit in 20 µl of final reaction per well following the manufacturer ratios using a StepOnePlus™ Real-Time PCR System.

2.9 | In situ hybridization

Digoxigenin RNA probes were synthesized using the Sp6/T7 Transcription Kit (Roche; see Supporting Information Table S2).

Adult and 3-month-old clownfishes were euthanized in MS222 at 200 mg/L. For each clownfish, the skin was dissected in a way to get in a same sample a part of the white body bar, the black bar, and the orange skin (posterior to the white body bar; Figure 4a). Adult skin samples were then fixed 24 hr in 4% paraformaldehyde diluted in PBS (phosphate-buffered saline). Samples were subsequently dehydrated stepwise in PBS/ethanol, and then put four times 10 min in butanol 100% and finally embedded in paraffin overnight. Embedded skin samples were sectioned transversally with a thickness of 8 µm using Leica Biosystems RM2245 Microtome. The samples were then treated as in Thisse, Thisse, Schilling, and Postlethwait (1993).

2.10 | Pharmacological treatments

TAE684 (NVP-TAE684; HY-10192, MedChem Express), a specific inhibitor of Ltk and Alk (Colanesi et al., 2012; Fadeev, Krauss, Singh, & Nüsslein-Volhard, 2016; Galkin et al., 2007; Rodrigues, Yang, Nikaido, Liu, & Kelsh, 2012), was diluted in dimethyl sulfoxide (DMSO; Sigma-Aldrich, Louis, MI, USA) to a final concentration of 6 mM. Clownfish juveniles were treated in 0.005% DMSO with 0.6 µM TAE684 or without (controls). For each condition, three juveniles were treated in 2 L fish medium in a beaker. Four hundred milliliter solution was changed every day.

2.11 | F_0 CRISPR/Cas9 mutagenesis and iridophore counts

Wild-type strain ABb zebrafish (a derivative of inbred Ab^{WP}; Eom et al., 2015) were housed under standard conditions. Embryos were injected with T7-transcribed single-guide RNAs (sgRNAs) and Cas9 protein as described (Shah, Davey, Whitebirch, Miller, & Moens, 2015). sgRNA protospacers were modified to "g" at 1st and 2nd 5′ positions to facilitate in vitro transcription as necessary. To increase likelihoods of biallelic knockdown, two sgRNAs were designed to target an early exon for each candidate gene. Embryos were injected at the one cell stage except for *fhl2a* and *fhl2b*, for which embryo survival was <10% at 4 days post-fertilization (dpf); sgRNAs targeting these loci were therefore injected into a single blastomere after early cytoplasmic bridges had closed (late 16–32 cell stage; Kimmel, Ballard, Kimmel, Ullmann, & Schilling, 1995) to diminish the numbers of clonal lineages carrying mutations and enhance survivorship. Mutagenicity of each sgRNA was confirmed by Sanger sequencing of amplicons from whole embryo genomic DNA. sgRNA targets are described in Supporting Information Table S4. F_0 embryos were raised at ~28°C for 4 days at which time larvae were anesthetized with MS222 and iridophores at the dorsal midline were counted manually under incident light. Analyses of iridophore counts were performed using JMP 14.0 statistical software (SAS Institute, Cary, NC, USA).

2.12 | RNA-Seq library preparation and sequencing

Information on sequencing methods as well as average read number and quality per sample is provided in Supporting Information Table S6.

3 | RESULTS

3.1 | White pigment cells in *Amphiprion ocellaris* are morphologically similar to iridophores

To determine the type of pigment cell responsible for the white color of *A. ocellaris* bars, we first compared white and orange skins microscopically. Both classical types of reflecting pigment cells known in vertebrates, leucophores and iridophores, can be distinguished by two main criteria: Iridophores are generally round and contain flattened reflecting platelets, and leucophores are dendritic with smaller and rounded organelles (Fujii, 1993; Schartl et al., 2015). Using light microscopy, we observed a white matte coloration overall within which scattered, rounded iridescent cells and dendritic melanophores could be observed occasionally. Given the apparent density of cells contributing to the white

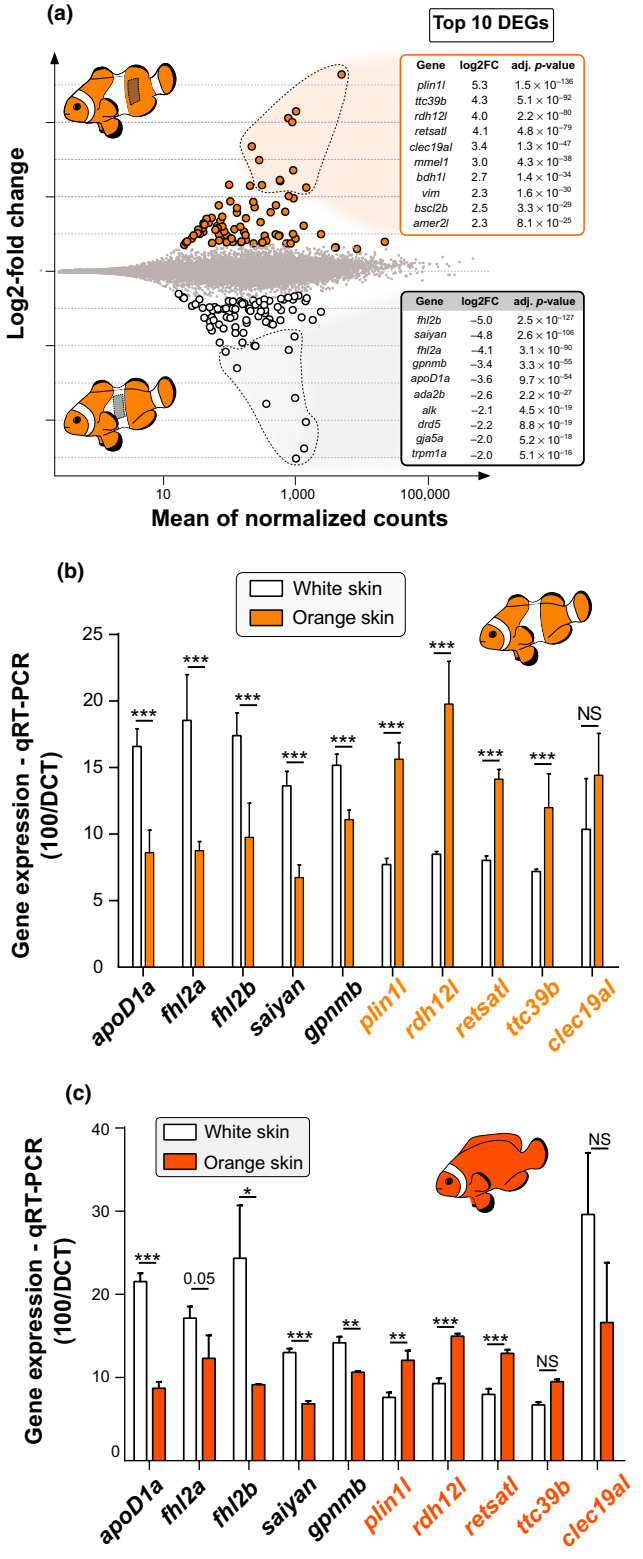

FIGURE 3 *fhl2a*, *fhl2b*, *apoD1a*, *saiyan*, and *gpnmb* are differentially expressed in the white skin. (a) Volcano plot comparing the orange and white skin transcriptomes in *Amphiprion ocellaris*. Statistically DEGs (FDR < 0.05, Benjamini–Hochberg correction) are highlighted compared to background genes. Insets indicate the 10 most significant genes in each condition (dashed area). (b) Histogram representing the relative gene expression determined by qPCR of *fhl2a*, *fhl2b*, *saiyan*, *gpnmb*, and *apoD1a* (*y*-axis) in white skin (white bar) compared to orange skin (orange bar) in independent *A. ocellaris* skins. (*t* test; ***$p < 0.0005$). (c) Histogram representing the relative gene expression determined by qPCR in white (white bar) compared to orange skin (orange bar) in *Amphiprion frenatus* (*t* test; *$p < 0.05$, **$p < 0.005$, ***$p < 0.0005$). [Colour figure can be viewed at wileyonlinelibrary.com]

matte color itself, individual pigment cells contributing to it were not discernable by light microscopy (Figure 1a). We therefore used transmission electron microscopy (TEM) to understand the nature of the white coloration. In the skin, the epidermis covers the scales whose ends lie inside the dermal tissue that contain the pigment cells (Figure 1b,d; Hirata et al., 2003). Within the dermis, pigment cells were abundant in the stratum laxum, which surrounds the inner and outer faces of the bony scales (Figure 1b,d, Sire, 1988). In skin from regions with white bars, the overwhelming majority of pigment cells had rounded bodies and contained oblong, ca. 0.5 µm platelets arranged parallel to one another in discrete stacks organized concentrically around the nucleus (Figure 1c and inset). The morphology and organization of these platelets were consistent with the cells being iridophores, which appear iridescent when platelets are precisely organized or white when platelets are less organized (Fujii, 1993; Schartl et al., 2015). Melanophores were observed occasionally as well. Although sparsely distributed iridescent cells were evident by light microscopy (Figure 1a), we were unable to identify a distinct population by TEM that might correspond to these cells, either because their features could not be distinguished from other pigment cells ultrastructurally, or, more likely, because they occur at densities too low to have been sampled in thin sections. Given that all unmelanized pigment cells in white bars were of a rounded (rather than dendritic) morphology and contained flattened (rather than rounded) organelles similar to those of iridophores, we conclude that white coloration of *A. ocellaris* is likely conferred by iridophores, rather than leucophores. In orange skin, we found no platelet-containing cells and observed instead only elongated xanthophores and melanophores (Supporting Information Figure S1).

3.2 | Comparative transcriptomics of orange versus white bars

To identify gene expression signatures specific to white and orange skin and their associated pigment cells, we generated transcriptomes from skin samples of each type from each of three adult *A. ocellaris* (Supporting Information Figure S2), using a reference transcriptome as well as whole genome data for *A. ocellaris* generated for comparative analyses (A. Marcionetti and N. Salamin, in preparation). Principal component analysis confirmed overall differences in gene expression between white and orange skin samples (axis 1, 41% of the variance; Supporting Information Figure S3). Individuals also differed markedly from one another at the transcriptomic level, which is not surprising given that individual fish were of heterogeneous, rather than inbred, genetic backgrounds (axis 2, 35% of the variance; Supporting Information Figure S3). Comparison of white and

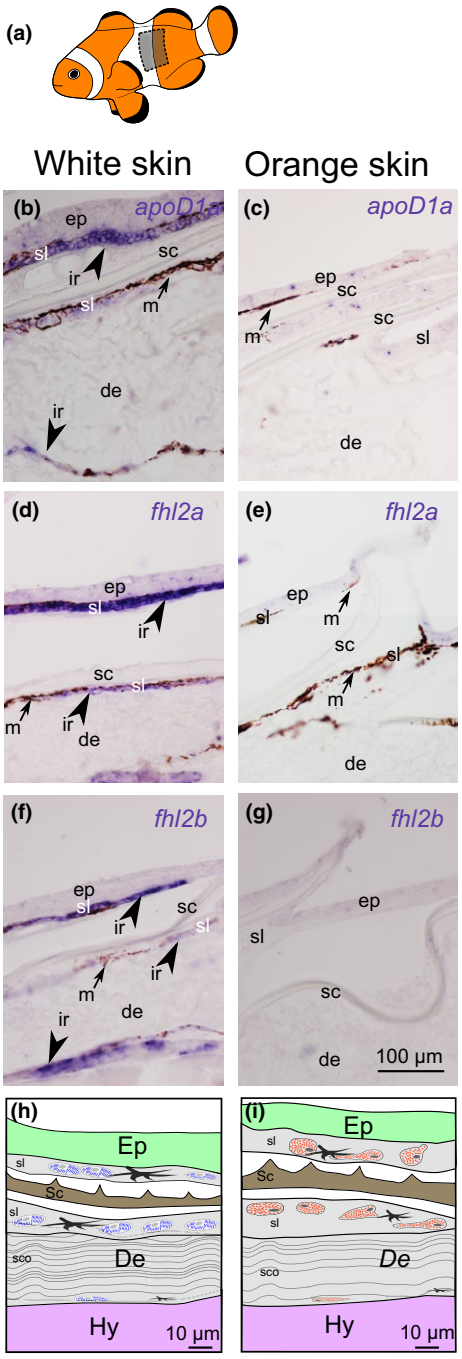

FIGURE 4 *fhl2a*, *fhl2b*, *apoD1a* are specifically expressed in iridophores within skin. (a) For in situ hybridization experiments, skin area was dissected in a way that each sample consistently included both prospective white and orange skin (white body bar and posterior orange skin; gray rectangle). The skin was then cut transversally using microtome to locate the expression of genes in the different skin layers. (b–g) In situ hybridization for transcript of *apoD1a* (b, c), *fhl2a* (d, e), *fhl2b* (f, g) in transverse sections of white (b, d, and f) and orange skins (c, e, and g) of *A. ocellaris* adults. (h, i) Cartoon of a transverse section of white (h) and orange skin (i). *de*: dermis; *ep*: epidermis; *hy*: hypodermis; *ir*: iridophores; *m*: melanophores; *sc*: scale; *sco*: *stratum compactum*; *sl*: *stratum laxum*. ISH experiments have been replicated in four individuals [Colour figure can be viewed at wileyonlinelibrary.com]

orange skin samples revealed 86 genes expressed at significantly higher levels in white skin and 83 genes expressed at significantly higher levels in orange skin ($p < 0.05$; Benjamini–Hochberg adjusted *p*-value; Supporting Information Table S3).

Skin samples include pigment cells and a variety of other cell types. To gain further insight into the transcriptomic signature of *A. ocellaris* white skin, we compared our results to an available set of 346 genes specifically enriched in zebrafish iridophores (Higdon, Mitra, & Johnson, 2013). Of these 346 loci, 237 were detectable in *A. ocellaris* skin samples (Supporting Information Table S5). Using this dataset, we carried out two types of analysis: (a) we first performed a gene set enrichment analysis using all *A. ocellaris* genes detectably expressed in both sample types. The expression levels of all genes were correlated to one or the other skin color. Each gene in the "iridophore gene set" (i.e., the clownfish orthologs of 237 zebrafish iridophore markers) was then ranked among all expressed genes ("Ranked gene list" in Supporting Information Figure S4a). The results show that the expression of the genes in this gene set is overall correlated to the white skin phenotypic information. Hence, a negative enrichment score is observed. The zebrafish iridophore gene set is thus enriched in white skin (*p*-value <0.01, 1,000 permutations); (b) second, we compared the zebrafish iridophore gene set to the 86 *A. ocellaris* genes expressed at significantly higher levels in white skin than in orange skin (Supporting Information Table S3). This comparison revealed 12 genes in common between *A. ocellaris* white skin and zebrafish iridophores, but only one gene between *A. ocellaris* orange skin and zebrafish iridophores (Supporting Information Figure S4b), a difference significantly greater than expected by chance (chi-square test, $p < 1e\text{-}16$).

Included among these 12 genes were four genes inferred previously to function in iridophore development, or likely to do so, including genes encoding products involved in the synthesis of purines, crystals present in iridophore reflecting platelets conferring their iridescence or white coloration (Fujii, 1993). For example, *pnp4a* encodes an enzyme required for purine synthesis mutated in the medaka iridophore mutant *guanineless* (Kimura et al., 2017) and is used as a marker of iridophores in zebrafish (Eom et al., 2015; Patterson & Parichy, 2013), whereas *prtfdc1* encodes an enzyme whose human ortholog is involved in purine metabolism (Welin et al., 2010). *tfec* encodes a basic helix–loop–helix transcription factor that marks the embryonic iridophore lineage in zebrafish (Lister, Lane, Nguyen, & Lunney, 2011) and *fhl2a* is a teleost-specific duplicate of *fhl2b*, encoding a four-and-half LIM domain transcription factor that has been recruited evolutionarily for iridophore-containing ornamental "eggspots" on the fins of cichlids (Santos et al., 2014).

Only one gene in the zebrafish iridophore gene set was found among the 83 DEGs in orange skin (Supporting Information Figure S4b): *fmn2*, encoding a formin protein, with no known pigmentation function (Higdon et al., 2013). We conclude that white bar pigment cells in *A. ocellaris* share similarities with iridophores at a gene expression level. Moreover, the genes differentially expressed in the orange skin provide a clear signature of xanthophores and could therefore be a useful resource to study this cell type in clownfish (not shown).

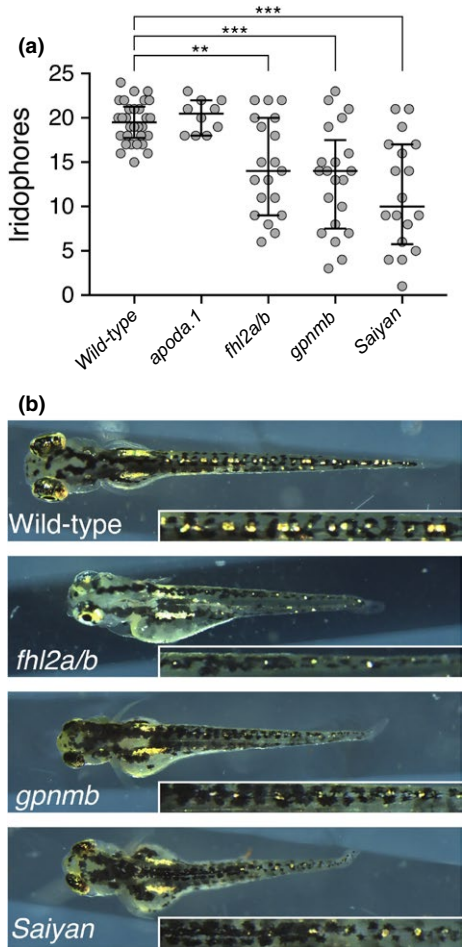

FIGURE 5 *fhl2a*, *fhl2b*, *saiyan*, and *gpnmb* are essential for development of iridophores in zebrafish. (a) Quantification of dorsal iridophores in zebrafish 4 dpf larvae. Each dot corresponds to one individual. Asterisks indicate significant differences in iridophores complements (non-parametric comparisons with control using Steel method; $^{**}p < 0.01$, $^{***}p < 0.001$). Although sizes differed between larvae that were controls and those that carried somatically induced mutations, these differences in length did not themselves account for variation in iridophore numbers as indicated by preliminary analysis of covariance that identified significant overall differences among groups ($F_{4,88} = 4.13$, $p < 0.005$) even after controlling for potential overall effects of standard length ($F_{1,88} = 0.05$, $p = 0.8$), as well as potential genotype × standard length interaction ($F_{4,88} = 1.18$, $p = 0.3$; using inverse-transformed counts to normalize residuals to meet model assumptions). (b) Typical phenotypes of uninjected controls and individuals mosaic for somatically induced mutations, with insets to illustrate dorsal iridescent iridophores used in analyses. In wt individuals, numerous iridophores (located with the arrowhead) were present along dorsal midlines, whereas injected individuals had fewer iridophores even after controlling for differences in body length [Colour figure can be viewed at wileyonlinelibrary.com]

3.3 | Iridophores are important for white color formation

We then used a pharmacological approach to test whether cells related to iridophores are responsible for white coloration in clownfish. In zebrafish, iridophores require leukocyte tyrosine kinase (Ltk) signaling (Lopes et al., 2008) and iridophores are ablated when fish are treated with TAE684 (TAE; Colanesi et al., 2012; Fadeev et al., 2016; Rodrigues et al., 2012), an inhibitor of Ltk and anaplastic lymphoma kinase (Alk). Transcriptomic data from white skin of *A. ocellaris* revealed expression of both *alk* and *ltk*, with *alk* being over-expressed in white skin compared to orange skin (Supporting Information Table S3). *A. ocellaris* juveniles treated with 0.6 μM TAE (in DMSO) for 16 days (20 until 36 dph) had reduced white coloration compared to controls (Figure 2a, arrowheads). In treated fish, white color was less intense and features beneath the integument (light myotomes on the trunk, reddish viscera anteriorly) were more visible. To confirm that reduced white coloration of the body bar in TAE-treated fishes was attributable to a reduction in iridophore number, we examined by TEM thin sections of white skin from control (DMSO) and 0.6 μM TAE684-treated fishes. These sections revealed dramatically fewer iridophores in TAE-treated fish compared to controls and a corresponding decrease in the depth of the stratum laxum where iridophores are normally found (Figure 2a, lower, white arrowheads). These observations indicate that cells visible by TEM that resemble iridophores are sensitive to a drug known to target iridophores and are indeed responsible for the white color.

To further validate the link between iridophores and white color, we tested whether TAE treatment was reversible. We treated *A. ocellaris* larvae from 5 to 20 dph with 0.6 μM TAE and observed the lack of the posterior and body bars and an anterior body bar formed but deficient in white coloration (Figure 2b). We then separated fish into two conditions: either continuing TAE treatment at 0.6 μM (TAE/TAE) or rearing in DMSO alone (TAE/DMSO; Figure 2b). After 16 additional days, individuals maintained in TAE lacked most of their posterior bars and had anterior bar deficient in white coloration. Fish shifted to DMSO after early TAE treatment regained stronger coloration in previously developed anterior bars, but failed to develop posterior bars (Figure 2b). Interestingly even 2 months after the treatment, posterior bars did not appear and were not subsequently observed throughout the life of the fish. Taken together, our observations show that white bars contains iridophores and strongly suggest that iridophores are themselves responsible for establishing color pattern and maintaining the prominent white coloration of the clownfish white bar.

3.4 | *fhl2a*, *fhl2b*, *saiyan*, *gpnmb*, and *apoD1a* are differentially expressed in white skin and iridophores

To validate transcriptomic results, we assessed by qRT-PCR the expression of five genes identified as most differentially expressed between white and orange skin on independent skin samples in *A. ocellaris* (Figure 3). For each locus, the directionality of the difference in expression was concordant between RNA-Seq and qRT-PCR (Figure 3b). The only exception was clec19a for which the expression difference was non-significant. Moreover, to test the generality of these results we also examined expression in a second *Amphiprion*

species. In *A. frenatus*, whose adults contain a unique white bar positioned on the head (Salis et al., 2018) on a dark reddish background, we found that white and orange skin genes were also differentially expressed as in *A. ocellaris*, with the exception of *ttc39b* (Figure 3c).

Among the 86 genes more highly expressed in white skin than orange skin, *fhl2a* and *fhl2b*—already known to be expressed in iridophores (Santos et al., 2014)—and *gpnmb* had higher expression in zebrafish iridophores than melanophores (Higdon et al., 2013). Apolipoprotein D (*apoD1a*) is expressed specifically in cichlids eggspots but its function in pigmentation, if any, has not been characterized (Gu & Xia, 2017). Finally, the gene with the second highest change in white skin was an ortholog to zebrafish gene ENSDARG00000055172 (Ensembl)/795494 (NCBI; Figure 3a) with no associated function in Ensembl, NCBI, or ZFIN databases. This gene is currently annotated as *si:ch211-256m1:8*, and we refer to it as *saiyan* in reference to the manga comics characters that can become shiny.

White bars appear late during post-embryonic development, starting at stage 4 and being well visible at stage 6 (N. Roux, P. Salis, and V. Laudet, in preparation; Salis et al., 2018). To test for an association between expression of these five genes and bar ontogeny, we used a transcriptomic dataset for skins across multiple post-embryonic stages. As shown in Supporting Information Figure S5, all five genes had minima of expression prior to overt bar development at stage 4, followed by increases through the climax of bar development at stage 6 and drops in expression by early juvenile stage 7.

To assess the spatial localization of these transcripts and confirm the presence of all five genes in iridophores, we performed in situ hybridization on *A. ocellaris* white and orange adult skin. *fhl2a*, *fhl2b*, and *apoD1a* were expressed in the stratum laxum of the dermis, mainly composed of iridophores as observed in Figure 1b, suggesting that those genes are effectively expressed in iridophores (Figure 4b,d,f, arrowheads). None of those three genes were expressed in orange skin sections (Figure 4c,e,g), and no signal was observed with the sense probes in the white sections (Supporting Information Figure S6). In contrast, we could not detect a clear difference in expression by in situ hybridization between white and orange skins for *saiyan* and *gpnmb* (not shown). To confirm the association of *fhl2a*, *fhl2b*, and *apoD1a* with iridophores, we looked at their expression in TAE-treated fishes in which no iridophores were observed (Figure 2a). Interestingly, those genes are not anymore expressed in the white skin of fishes treated for 20 days in TAE 0.6 μM (Supporting Information Figure S7).

Taken together, these data show that at least the three genes *fhl2a*, *fhl2b*, and *apoD1a* are specifically expressed in iridophores.

3.5 | *fhl2a*, *fhl2b*, *saiyan*, and *gpnmb* are required for iridophore development in zebrafish

To test whether *fhl2a*, *fhl2b*, *apoD1a*, *gpnmb*, and *saiyan* are essential for iridophore development, we assayed their function in zebrafish. We predicted that if these genes are required for iridophore lineage, then loss of function mutations should result in iridophore deficiencies at early stages. Accordingly, we generated fish mosaic (F_0) for somatically induced CRISPR/Cas9 mutations and compared the numbers of dorsal iridophores that developed with those of wild-type sibling controls. Given that *fhl2a* and *fhl2b* are paralogous loci, we tested their effects simultaneously. At 4 days post-fertilization, fish mosaic for mutations in *apoda.1* (*apoD1a* clownfish ortholog) did not have iridophore defects but those harboring mutations in *fhl2a/fhl2b*, *gpnmb*, and *saiyan* exhibited significantly fewer iridophores than uninjected siblings, even after controlling for variation in standard length (Figure 5). Thus, most of those DEG genes in *A. ocellaris* white skin were required for early iridophore development in zebrafish, consistent with *A. ocellaris* pigment cells of white skin representing a specific class of iridophore required for generating the striking white bars of clownfish.

4 | DISCUSSION

Our findings suggest that clownfish have iridophores enriched in white bars and that these cells are critically important in producing the white color, though we cannot formally exclude contributions of other mechanisms or cell types (e.g., dermal cells of the stratum laxum).

First, microscopic analyses showed that cells with a typical iridophore morphology (round shape cells with flattened reflecting platelets) were abundant in white bars (Figure 1; Fujii, 1993; Schartl et al., 2015). The iridophores in clownfish white bars were similar to zebrafish S-type iridophores that contain densely stacked purine platelets with a platelet size of ca. 0.5–2 μm, as compared to L-iridophores that have larger purine platelets (ca. 10 μm) organized parallel to the dermis (Hirata et al., 2003). This latter type was not observed. The relationship between the iridescent cells that we see in light microscopy and the iridophores that we see in electron microscopy—likely responsible for the white color—is still unclear. The radial arrangement of iridophore platelets observed in TEM is a likely contributor to the matte appearance (Fujii, 1993). However, we have not seen in our sections iridophores with a parallel or at least non-radial organization that would contribute to Tyndall scattering required for iridescence. Therefore, future work should clarify the existence of possible subtypes among clownfish iridophores.

Second, using transcriptomic analysis, we independently confirmed that cells with transcriptional profiles similar to iridophores contribute to white but not orange skin (Figure S4). We compared genes specific to zebrafish iridophores (Higdon et al., 2013) with genes differentially expressed in clownfish white skin and showed that overlap between datasets was significantly greater than would be expected by chance, showing that white skin in clownfish had a transcriptomic signature of iridophores. In particular, 12 genes were common to both datasets and could thus constitute conserved iridophore markers within actinopterygians. Although significant, this overlap was relatively small compared to the size of respective

clownfish (86) and zebrafish sets of genes (237). This presumably reflects differences in sample origins: Zebrafish RNA-Seq data were obtained from purified iridophores, whereas clownfish data were derived from whole skin in which many other cell types are present (Higdon et al., 2013). Thus, clownfish data represented a more diverse set of cells compared to the zebrafish dataset, though biological species differences in iridophore transcriptomes may also explain some of the differences between both datasets. These and other possibilities will be resolvable with transcriptomic profiling of purified populations of clownfish iridophores.

Third, we retrieved previously identified iridophore markers in the list of the most DEGs in white skin (Figure 3). Among the 12 genes found in common between the clownfish white bar and zebrafish iridophores, 4 (*pnp4a*, *prtfdc1*, *tfec*, and *fhl2a*) were already demonstrated or inferred to be important for the development or function of iridophores in teleost fishes (Kimura et al., 2017; Lister et al., 2011; McMenamin et al., 2014; Petratou et al., 2018; Santos et al., 2014; Welin et al., 2010).

Fourth, our pharmacological experiments showed that treatment with TAE 684, an inhibitor of Ltk and Alk tyrosine kinase receptors expressed by zebrafish iridophores (Colanesi et al., 2012; Fadeev et al., 2016, 2018; Lopes et al., 2008; Rodrigues et al., 2012), reduced the number of presumptive iridophores at an ultrastructural level and concomitantly reduced the white hue of the bars at the organismal level (Figure 2). Both *alk* and *ltk* were expressed in cells of white skin, *alk* being more highly expressed in white skin than orange skin (Supporting Information Table S3). Therefore Ltk, Alk, or both are required for iridophores. Here, we extended previous analyses by showing that TAE 684 treatment affects iridophores and the white hue of juvenile fish even after bars have formed (Salis et al., 2018). Interestingly, early blockade of bar formation prevented subsequent normal development of posterior bars, but not the most anterior ones (Figure 2b). Moreover, anterior bars that had developed during early TAE treatment were able to regenerate a nearly normal white appearance after removal of TAE, whereas posterior bars that failed to develop initially under these conditions also failed to develop subsequently. Anterior–posterior differences in TAE sensitivity suggest intrinsic differences between bars, and perhaps distinct Ltk- or Alk-mediated processes, worthy of further investigation.

Fifth, we found that zebrafish with somatic mutations in orthologs of three to four genes most differentially expressed in clownfish white skin had significantly fewer iridophores compared to controls (Figure 5). Owing to the mosaicism of these F_0 fish, it is likely that not all cells carried mutant alleles and so these analyses likely underestimate the magnitude of phenotypic effects attributable to loss of function mutations. Among the genes tested (*fhl2a* and *2b* being tested together because of their sequence relatedness), only one (*apoda.1*) failed to generate a clear phenotype.

Lastly, our data are not consistent with clownfish white skin pigment cells being leucophores, as opposed to iridophores. Leucophores are dendritic cells with round organelles that lack an overt organization (Schartl et al., 2015), distinct from the round cells with flat, highly organized organelles that we observed in clownfish. To date, only one gene, *slc2a15b*, has been documented to have expression specific to leucophores (Kimura et al., 2014). This gene was not expressed detectably in clownfish skin samples, whereas its teleost-specific paralog, *slc2a15a*, was expressed at comparable levels between white and orange skin. Eventual identification of additional leucophore-specific markers will enable future studies of these questions.

The comparison of white and orange colored skin provided a set of genes differentially expressed in each condition, some of which might constitute new iridophore and xanthophore markers. Among the 10 most DEGs in clownfish white bar, four were previously associated with confirmed or putative iridophore differentiation processes: *fhl2a* and *fhl2b*, *tfec*, and *gpnmb*. As discussed above, *fhl2* genes were associated with iridophores found in cichlid egg-spots (Santos et al., 2014) and were expressed in zebrafish iridophores (Higdon et al., 2013). *Gpnmb* was also expressed in iridophores of zebrafish (Higdon et al., 2013) and cichlids (Santos et al., 2014).

Among the 10 most DEGs in white skin, we identified two other genes (*gja5* and *trpm1a*) associated with pigmentation although not necessarily in iridophores. Mutations in *gja5* result in the zebrafish *leopard* mutant phenotype, characterized by a spotted pattern (Irion et al., 2014; Watanabe et al., 2006). In addition, we identified several genes that, to our knowledge, have not been previously assigned roles in pigmentation. Three of those (*ada2*, *prtfdc1*, and *slc2a9*) are involved in purine metabolism (Pei et al., 2016; Welin et al., 2010), consistent with a function in platelet formation.

Ranked second within the most DEGs in white skin was *saiyan* also identified in the comparison between both zebrafish and iridophore datasets. Its role in iridophore development was functionally confirmed in zebrafish, as mosaic CRISPR/Cas9 F_0 fish mosaic for *saiyan* mutations harbored ~40% fewer iridophores compared to wild type (Figure 5).

5 | CONCLUSION

We have shown that the white color of an iconic fish species, the clownfish *A. ocellaris*, is composed of iridophores, and we identified several new genes of likely importance to the development or maintenance of these cells. This analysis opens the door to functional analyses of the extraordinarily diverse pigmentation patterns of coral reef fishes and will allow for integrated studies relating developmental genetics and evolution of pattern formation to the fascinating behaviors and ecologies of these fishes.

6 | DATA AVAILABILITY

Data are available at NCBI (SRA database) under BioProject PRJNA482393 and BioProject PRJNA482578. Scripts used to generate the transcriptomic results and phylogenetic trees are availableathttp://igfl.ens-lyon.fr/equipes/j.-n.-volff-fish-evolutionary-genomics/lorin_additional_data/salis_lorin_pigmentation_skin_aocellaris/salis_lorin_supp-trees-top-degs.

ACKNOWLEDGEMENTS

TL holds a grant from the French MENRT. We thank Bruno Frédérich for critical reading. We thank the OOB's Bio2Mar and Biopic platforms for technical help. Clownfish husbandry was supported by the CNRS Interdisciplinarity Actions and EMBRC-France (ANR-10-INBS-02). Additional support was provided by NIH R35 GM122471 to D.M.P.

CONFLICT OF INTEREST

The authors declare no conflict of interest.

AUTHORS' CONTRIBUTIONS

P.S. achieved all the experiments concerning RNA extraction, stereomicroscope experiments, ISH, TAE treatments, and qRT-PCR. P.S. and M.-L.E. performed electron microscopy experiments. T.L., M.S., and C.R. implemented transcriptomic analysis using an *A. ocellaris* genome sequenced by A.M., N.S., N.R., and L.B. provided help for specific experiments on *A. ocellaris*. V.L. performed CRISPR/CAS9 experiments in zebrafish. P.S., T.L., D.P., and V.L. designed the study. P.S., V.L., T.L., J.-N.V., and D.P. wrote the article.

ORCID

Vincent Laudet https://orcid.org/0000-0003-4022-4175

REFERENCES

Anisimova, M., Gil, M., Dufayard, J. F., Dessimoz, C., & Gascuel, O. (2011). Survey of branch support methods demonstrates accuracy, power, and robustness of fast likelihood-based approximation schemes. *Systematic Biology*, *60*, 685–699. https://doi.org/10.1093/sysbio/syr041

Colanesi, S., Taylor, K. L., Temperley, N. D., Lundegaard, P. R., Liu, D., North, T. E., … Patton, E. E. (2012). Small molecule screening identifies targetable zebrafish pigmentation pathways. *Pigment Cell Melanoma Research*, *25*, 131–143. https://doi.org/10.1111/j.1755-148X.2012.00977.x

Cuthill, I. C., Allen, W. L., Arbuckle, K., Caspers, B., Chaplin, G., Hauber, M. E., … Caro, T. (2017). The biology of color. *Science*, *357*, eaan0221. https://doi.org/10.1126/science.aan0221

Djurdjevič, I., Kreft, M. E., & Sušnik Bajec, S. (2015). Comparison of pigment cell ultrastructure and organisation in the dermis of marble trout and brown trout, and first description of erythrophore ultrastructure in salmonids. *Journal of Anatomy*, *227*, 583–595. https://doi.org/10.1111/joa.12373

Eom, D. S., Bain, E. J., Patterson, L. B., Grout, M. E., & Parichy, D. M. (2015). Long-distance communication by specialized cellular projections during pigment pattern development and evolution. *Elife*, *4*, e12401. https://doi.org/10.7554/eLife.12401

Eom, D. S., & Parichy, D. M. (2017). A macrophage relay for long-distance signaling during postembryonic tissue remodeling. *Science*, *355*, 1317–1320. https://doi.org/10.1126/science.aal2745

Fadeev, A., Krauss, J., Singh, A. P., & Nüsslein-Volhard, C. (2016). Zebrafish Leucocyte tyrosine kinase controls iridophore establishment, proliferation and survival. *Pigment Cell Melanoma Research*, *29*, 284–296. https://doi.org/10.1111/pcmr.12454

Fadeev, A., Mendoza-Garcia, P., Irion, U., Guan, J., Pfeifer, K., Wiessner, S., …Palmer, R. H. (2018). ALKALs are in vivo ligands for ALK family receptor tyrosine kinases in the neural crest and derived cells. *Proceedings of the National Academy of Sciences of the United States of America*, *115*, E630–E638. https://doi.org/10.1073/pnas.1719137115

Frohnhöfer, H. G., Krauss, J., Maischein, H. M., & Nüsslein-Volhard, C. (2013). Iridophores and their interactions with other chromatophores are required for stripe formation in zebrafish. *Development*, *140*, 2997–3007. https://doi.org/10.1242/dev.096719

Fujii, R. (1993). Cytophysiology of fish chromatophores. *International Review of Cytology*, *143*, 191–255.

Galkin, A. V., Melnick, J. S., Kim, S., Hood, T. L., Li, N., Li, L., & …Warmuth, M. (2007). Identification of NVP-TAE684, a potent, selective, and efficacious inhibitor of NPM-ALK. *Proceedings of the National Academy of Sciences of the United States of America*, *104*, 270–275. https://doi.org/10.1073/pnas.0609412103

Grabherr, M. G., Haas, B. J., Yassour, M., Levin, J. Z., Thompson, D. A., Amit, I., … Regev, A. (2011). Full-length transcriptome assembly from RNA-Seq data without a reference genome. *Nature Biotechnology*, *29*, 644–652. https://doi.org/10.1038/nbt.1883

Gu, L., & Xia, C. (2017). Revelation of the genetic basis for convergent innovative anal fin pigmentation patterns in cichlid fishes. *bioRxiv*. in press.

Higdon, C. W., Mitra, R. D., & Johnson, S. L. (2013). Gene expression analysis of zebrafish melanocytes, iridophores, and retinal pigmented epithelium reveals indicators of biological function and developmental origin. *PLoS ONE*, *8*, e67801. https://doi.org/10.1371/journal.pone.0067801

Hirata, M., Nakamura, K., Kanemaru, T., Shibata, Y., & Kondo, S. (2003). Pigment cell organization in the hypodermis of zebrafish. *Developmental Dynamics*, *227*, 497–503. https://doi.org/10.1002/dvdy.10334

Irion, U., Frohnhöfer, H. G., Krauss, J., Çolak Champollion, T., Maischein, H. M., … Nüsslein-Volhard, C. (2014). Gap junctions composed of connexins 41.8 and 39.4 are essential for colour pattern formation in zebrafish. *Elife*, *3*, e05125.

Kim, D., Langmead, B., & Salzberg, S. L. (2015). HISAT: A fast spliced aligner with low memory requirements. *Nature Methods*, *12*, 357–360. https://doi.org/10.1038/nmeth.3317

Kimmel, C. B., Ballard, W. W., Kimmel, S. R., Ullmann, B., & Schilling, T. F. (1995). Stages of embryonic development of the zebrafish. *Developmental Dynamics*, *203*, 253–310. https://doi.org/10.1002/aja.1002030302

Kimura, T., Nagao, Y., Hashimoto, H., Yamamoto-Shiraishi, Y., Yamamoto, S., Yabe, T., … Naruse, K. (2014). Leucophores are similar to xanthophores in their specification and differentiation processes in medaka. *Proceedings of the National Academy of Sciences of the United States of America*, *111*, 7343–7348. https://doi.org/10.1073/pnas.1311254111

Kimura, T., Takehana, Y., & Naruse, K. (2017). pnp4a is the causal gene of the medaka iridophore mutant *guanineless*. *G3*, *7*, 1357–1363. https://doi.org/10.1534/g3.117.040675

Kopylova, E., Noé, L., & Touzet, H. (2012). SortMeRNA: Fast and accurate filtering of ribosomal RNAs in metatranscriptomic data. *Bioinformatics*, *28*, 3211–3217. https://doi.org/10.1093/bioinformatics/bts611

Li, H., Handsaker, B., Wysoker, A., Fennell, T., Ruan, J., Homer, N. … 1000 Genome Project Data Processing Subgroup (2009). The sequence alignment/map format and SAMtools. *Bioinformatics*, *25*, 2078–2079.

Lister, J. A., Lane, B. M., Nguyen, A., & Lunney, K. (2011). Embryonic expression of zebrafish MiT family genes tfe3b, tfeb, and tfec. *Developmental Dynamics*, *240*, 2529–2538. https://doi.org/10.1002/dvdy.22743

Lopes, S. S., Yang, X., Müller, J., Carney, T. J., McAdow, A. R., Rauch, G. J., … Kelsh, R. N. (2008). Leukocyte tyrosine kinase functions in

pigment cell development. *PLoS Genetics*, *4*, e1000026. https://doi.org/10.1371/journal.pgen.1000026

Lorin, T., Brunet, F. G., Laudet, V., & Volff, J. N. (2018). Teleost Fish-Specific Preferential Retention of Pigmentation gene-containing families after whole genome duplications in vertebrates. *G3*, *8*, 1795–1806. https://doi.org/10.1534/g3.118.200201

Love, M. I., Huber, W., & Anders, S. (2014). Moderated estimation of fold change and dispersion for RNA-seq data with DESeq2. *Genome Biology*, *15*, 550. https://doi.org/10.1186/s13059-014-0550-8

McMenamin, S. K., Bain, E. J., McCann, A. E., Patterson, L. B., Eom, D. S., Waller, Z. P., … Parichy, D. M. (2014). Thyroid hormone-dependent adult pigment cell lineage and pattern in zebrafish. *Science*, *345*, 1358–1361. https://doi.org/10.1126/science.1256251

Nagao, Y., Suzuki, T., Shimizu, A., Kimura, T., Seki, R., Adachi, T., … Hashimoto, H. (2014). Sox5 functions as a fate switch in medaka pigment cell development. *PLoS Genetics*, *10*, e1004246. https://doi.org/10.1371/journal.pgen.1004246

Nagao, Y., Takada, H., Miyadai, M., Adachi, T., Seki, R., Kamei, Y., … Hashimoto, H. (2018). Distinct interactions of Sox5 and Sox10 in fate specification of pigment cells in medaka and zebrafish. *PLoS Genetics*, *14*, e1007260. https://doi.org/10.1371/journal.pgen.1007260

Nakamasu, A., Takahashi, G., Kanbe, A., & Kondo, S. (2009). Interactions between zebrafish pigment cells responsible for the generation of Turing patterns. *Proceedings of the National Academy of Sciences of the United States of America*, *106*(21), 8429–8434. https://doi.org/10.1073/pnas.0808622106

Patterson, L. B., & Parichy, D. M. (2013). Interactions with iridophores and the Tissue Environment required for patterning melanophores and xanthophores during zebrafish adult pigment stripe formation. *PLoS Genetics*, *9*, e1003561. https://doi.org/10.1371/journal.pgen.1003561

Pei, W., Xu, L., Varshney, G. K., Carrington, B., Bishop, K., Jones, M., … Burgess, S. M. (2016). Additive reductions in zebrafish PRPS1 activity result in a spectrum of deficiencies modeling several human PRPS1-associated diseases. *Scientific Reports*, *6*, 29946. https://doi.org/10.1038/srep29946

Petratou, K., Subkhankulova, T., Lister, J. A., Rocco, A., Schwetlick, H., & Kelsh, R. N. (2018). A systems biology approach uncovers the core gene regulatory network governing iridophore fate choice from the neural crest. *PLoS Genetics*, *14*(10), e1007402. https://doi.org/10.1371/journal.pgen.1007402

Rodrigues, F. S. L. M., Yang, X., Nikaido, M., Liu, Q., & Kelsh, R. (2012). A simple, highly visual in vivo screen for anaplastic lymphoma kinase inhibitors. *ACS Chemical Biology*, *7*, 1968–1974.

Salis, P., Roux, N., Soulat, O., Lecchini, D., Laudet, V., & Frédérich, B. (2018). Ontogenetic and phylogenetic simplification during white stripe evolution in clownfishes. *BMC Biology*, 16–90 in press. https://doi.org/10.1186/s12915-018-0559-7

Santos, M. E., Braasch, I., Boileau, N., Meyer, B. S., Sauteur, L., Böhne, A., … Salzburger, W. (2014). The evolution of cichlid fish egg-spots is linked with a cis-regulatory change. *Nature Communications*, *5*, 5149. https://doi.org/10.1038/ncomms6149

Schartl, M., Larue, L., Goda, M., Bosenberg, M. W., Hashimoto, H., & Kelsh, R. N. (2015). What is a vertebrate pigment cell? *Pigment Cell Melanoma Research*, *29*, 8–14. https://doi.org/10.1111/pcmr.12409

Shah, A. N., Davey, C. F., Whitebirch, A. C., Miller, A. C., & Moens, C. B. (2015). Rapid reverse genetic screening using CRISPR in zebrafish. *Nature Methods*, *12*, 535–540.

Singh, A. P., & Nüsslein-Volhard, C. (2015). Zebrafish stripes as a model for vertebrate colour pattern formation. *Current Biology*, *25*, 81–92. https://doi.org/10.1016/j.cub.2014.11.013.

Sire, J. Y. (1988). Evidence that mineralized spherules are involved in the formation of the superficial layer of the elasmoid scale in cichlids Cichlasoma octofasciatum and *Hemichromis bimaculatus* (Pisces, Teleostei): An epidermal active participation? *Cell Tissue Research*, *253*, 165–172.

Soneson, C., Love, M. I., & Robinson, M. D. (2015). Differential analyses for RNA-seq: transcript-level estimates improve gene-level inferences. *F1000Research*, *4*, 1521.

Subramanian, A., Tamayo, P., Mootha, V. K., Mukherjee, S., Ebert, B. L., Gillette, M. A., … Mesirov, J. P. (2005). Gene set enrichment analysis: A knowledge-based approach for interpreting genome-wide expression profiles. *Proceedings of the National Academy of Sciences of the United States of America*, *102*, 15545–15550. https://doi.org/10.1073/pnas.0506580102

Thisse, C., Thisse, B., Schilling, T. F., & Postlethwait, J. H. (1993). Structure of the zebrafish snail1 gene and its expression in wild-type, spadetail and no tail mutant embryos. *Development*, *119*, 1203–1215.

Watanabe, M., Iwashita, M., Ishii, M., Kurachi, Y., Kawakami, A., Kondo, S., & Okada, N. (2006). Spot pattern of leopard *Danio* is caused by mutation in the zebrafish connexin41.8 gene. *EMBO Reports*, *7*, 893–897. https://doi.org/10.1038/sj.embor.7400757

Watanabe, M., & Kondo, S. (2015). Is pigment patterning in fish skin determined by the Turing mechanism? *Trends in Genetics*, *31*, 88–96.

Welin, M., Egeblad, L., Johansson, A., Stenmark, P., Wang, L., Flodin, S., … Nordlund, P. (2010). Structural and functional studies of the human phosphoribosyltransferase domain containing protein 1. *FEBS Letters*, *277*, 4920–4930. https://doi.org/10.1111/j.1742-4658.2010.07897.x

SUPPORTING INFORMATION

Additional supporting information may be found online in the Supporting Information section at the end of the article.

How to cite this article: Salis P, Lorin T, Lewis V, et al. Developmental and comparative transcriptomic identification of iridophore contribution to white barring in clownfish. *Pigment Cell Melanoma Res*. 2019;32:391–402. https://doi.org/10.1111/pcmr.12766

SUPPLEMENTARY FIGURES

Supplementary Figure 1. Pigment cells organization in orange skin of *A. ocellaris*. **(A)** Stereomicroscope image of the orange skin shows melanophores and an orange coloration throughout which is due to xanthophores as shown with TEM magnification (**B- C**) (individual cells cannot be distinguished using stereomicroscope images). (**B-C**) TEM high magnification of xanthophores (arrowheads) (**B**) and xantosomes. (**D**) Cartoon representing a transversal section of the orange skin of *A. ocellaris* with xanthophores (represented by the orange cells) and melanophores (cells with stars shape). The majority of pigment cells are found in the stratum lexum of the dermis (grey).
M: melanophores, Xa: Xanthophores, Nu : nucleus, Sc: Scale, De: dermis, Hy: Hypodermis, Ep: Epidermis, BM: Basal Membrane, sl: stratum lexum, sco: stratum compactum

Supplementary Figure 2. Pipeline for transcriptomic analysis.

Supplementary Figure 3. (A) A schematic representation of the dissected area is shown (shaded areas). **(B)** PCA of data shows a separation between white and orange samples but a strong "individual" effect that we corrected for in DESeq2 using *indiv + color* as model.

Supplementary Figure 4. Transcriptomic analysis confirm that white cells are iridophores in *A. ocellaris*. **(A)** Gene Set Enrichment Analysis results for iridophores markers based on iridophore-specific RNA-Seq results (Higdon et al., 2013). This gene set is statistically enriched in the white skin ($P<0.01$, 1000 permutations). Each gene in the gene set is indicated by a vertical black bar. Colored squares indicate relatively high (red) or low (blue) expression in different samples for each marker. **(B)** 237 genes, markers of iridophores characterized in zebrafish (Higdon et al 2013), were compared to the lists of 86 white and 83 orange DEGs obtained in this study. There were 12 genes in common between the iridophore gene list and the 86 clownfish white DEGs (intersection is significant, *p*-value < 1e-16, chi2 test) but only 1 gene in common between the iridophore gene list and the 83 orange DEGs (not significant). Numbers indicate the number of genes in each area. Gene symbols in common between

datasets are indicated; numbers in bold indicate relative rank in the list of DEGs. For instance, *fhl2a* is the 3rd most significantly differentially expressed gene in white tissue (see Supplementary Table 3).

Supplementary Figure 5.

Normalized expression levels of top 5 white DEGs (blue= saiyan, green= apod1a, black= fhl2a, red= fhl2b, violet= gpnmb) along seven *A. ocellaris* developmental stages. For each DEGs, dots correspond to the expression level of one replicate normalized by the expression level of an arbitrary individual at stage S1 of the corresponding DEGs. Lines correspond to the mean values of normalized expression level of all replicates over the stages. Red arrow on individuals indicates the onset of white bar development.

Supplementary Figure 6.

In situ hybridization of sens probes of *fhl2a* (**A**), *fhl2b* (**B**), *apoD1a* (**C**), in transversal sections of white body bar of *A. ocellaris* adults. *ep* = epidermis, *sc* = scale, *de* = dermis, *ir* = iridophores. ISH experiments have been replicated in 4 individuals.

Supplementary Figure 7.

In situ hybridization of antisens probes of *fhl2a* (**A-B**), *fhl2b* (**C-D**), *apoD1a* (**E-F**), in transversal sections of white body bar of control (**A**, **C**, **E**) or TAE-treated (**B**, **D**, **E**) *A. ocellaris* adults. (*ep* = epidermis, *sc* = scale, *de* = dermis, *ir* = iridophores, m = melanophores). ISH experiments have been replicated in 4 individuals.

SUPPLEMENTARY TABLES

Supp. Table 1. qPCR primers

fhl2b-F	*TACTCTGCCAAGTGCCATGC*
fhl2b-R	*CAACGGTTGCAGGAGAAGCAG*
fhl2a-F	*TTTATGCCAAGAAGTGCGCCTC*
fhl2a-R	*ACTGGCGCTCCTCAAAGGAAATG*
apo D-F	*GTACTCTTGCACCGACATTCTGAGG*
apo D-R	*ATGGCTTTCTGGATGGTGGAGTC*
saiyan-F	*TGTTCGCTGCCAGCCGTATTC*
saiyan-R	*CAACAGGGAACACTCCTCTAACAC*
gpnmb-F	*TACCCACCGCTGAACCCAAAG*
gpnmb-R	*TTGGCAGTGAAGGTGATGCAGG*
plin1-F	*CAAGCCATGAGAAGGGCCAC*
plin1-R	*AGAGCATAACTGTTGGCGACG*
rdh12-F	*ATGGGCAAGATCCAGTTCGATG*
rdh12-R	*CTAGCTTGCTCTGTGCGTAGG*
retsat-F	*CAGGCTCTTTCTGCCTACCTGTTC*
retsat-R	*CACGCTTGTAGTGGTGGAGGAG*
ttc39b-F	*GATGGAGTTTCTGGGTTTCTCTGG*
ttc39b-R	*AGTCAGGGTGCTGAGGATGG*
clec19a-F	*AAGGGACTGACCAAAGGAGACG*
clec19a-R	*TGAACTTAGAGCCGTCGCTCC*
rpl32-F	*AACCAAGAAGTTCATTCGCCATCAG*
rpl32-R	*TGAGCATCTGACCCTTGAACC*

Supp. Table 2. ISH primers

fhl2b-HIS-F	*GGAGAACCTTCCCTACTGCA*
fjl2b-HIS-R	*CAGGGAAACGCAGCACTTTT*
fhl2a-HIS-F	*TGCTTCAAGTGCTTCCAGTG*
fhl2a-HIS-R	*AGATGTCCTTGCCACACTCT*
apo D-HIS-F	*GGGAGATGGTTTGAAATTGCC*
apo D-HIS-R	*GAATCATCCTGCTCACATCGA*
saiyan-HIS-F	*CAGACAGCCTTCATGCCATC*
saiyan-HIS-R	*CAAGCATCAAACAGGCCCTT*
gpnmb-HIS-F	*CCGCTGAACCCAAAGTCAAA*
gpnmb-HIS-R	*TTACCACCTGATTGCCGTCT*

Supp. Table 3. **Gene list of differentially expressed genes ranked by adjusted p-value significance.**

Positive log2-fold change values (in orange) correspond to genes overexpressed in orange skin. Negative log2-fold change values (in blue) correspond to genes overexpressed in white skin. For top DEGs, phylogenetic analyses were performed to ascertain gene naming. Base mean corresponds to average expression (in transcripts per million) over six samples.

Supp Table 4. List of the sg RNA used for CrispR/CAS9 knock-outs

*apoDa.1*_1 GGCACCTGGGCACTCATGAG;

*apoDa.1*_2 GgAGGTGTTTCTGGTCGTGT;

Saiyan_1 GgAGTACCCGGCTCGCCTCC*;*

Saiyan_2 GgGATCTGGCACAGATAGAG*;*

fhl2a_1 gGTAGCACTTCACACAGTAT*;*

fhl2a_2 GGGTTTCTTGCATTCCTCGC*;*

fhl2b_1 GGGCTTTTTGCACTCCTCGC*;*

fhl2b_2 gGGGAAGAAGTACGTCCTGC*;*

gpnmb_1 GGGAACCGGACACGAACCCT*;*

gpnmb_2 GGATACAGAGATTCGTCCCA.

Supp Table 5. List of the 237 loci that overlap between zebrafish iridophore markers and genes overexpressed in *Amphiprion ocellaris* white skin. For each gene, the gene symbol as annotated in NCBI is given (column 1) as well as the comprehensive NCBI gene description (column 2).

Supp Table 6. For each sample used in this study, sample type, replicate (individual) number, sequencing method (paired-end or single-end and reade length), total number of reads and % of bases having a quality score above 30 are indicated

Supplementary Figure 1

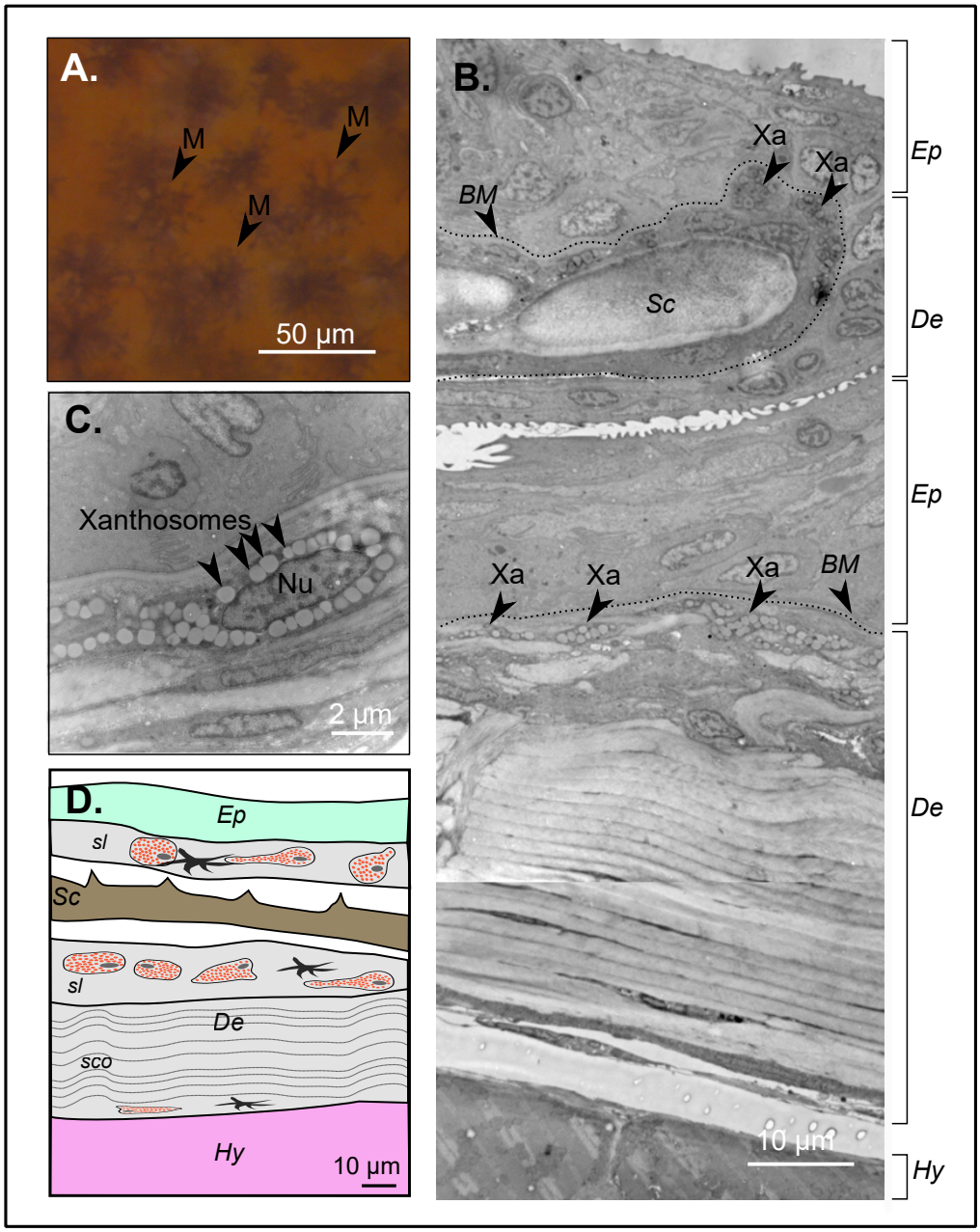

Supplementary Figure 2

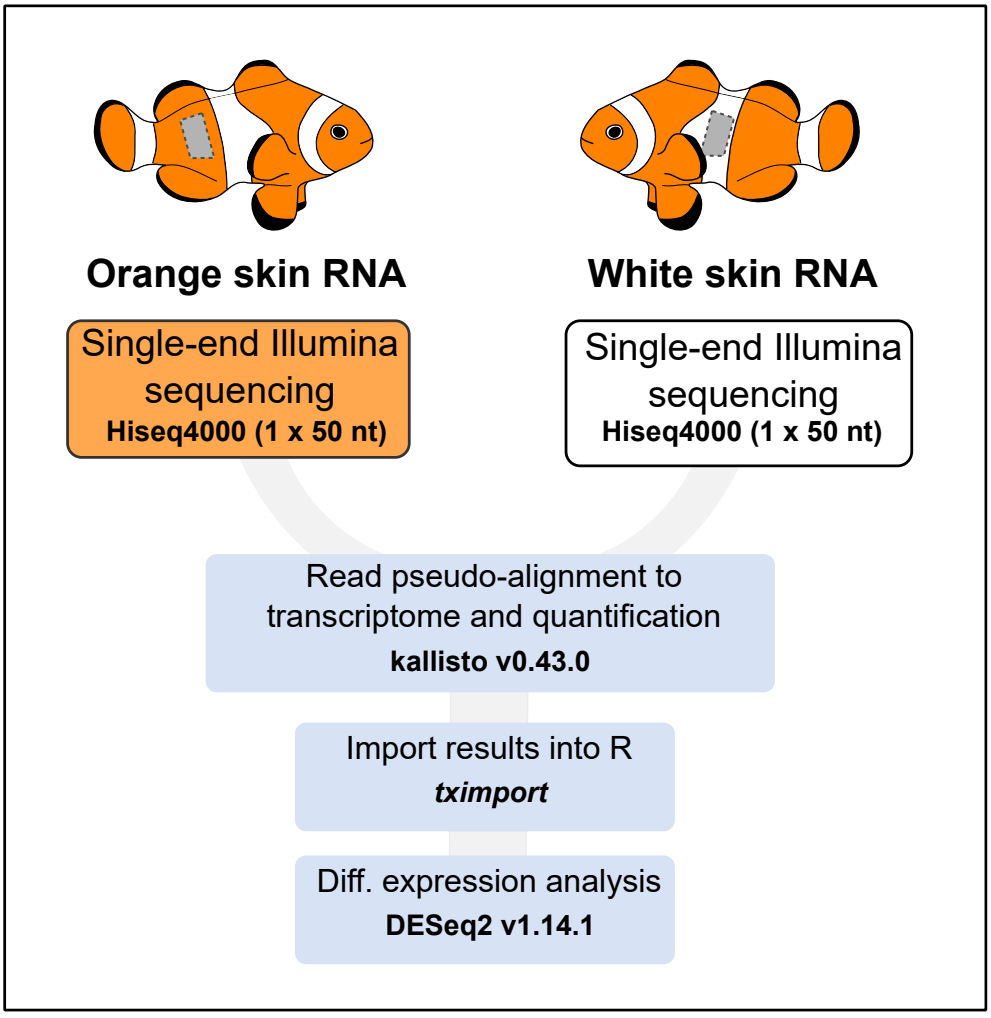

Supplementary Figure 3

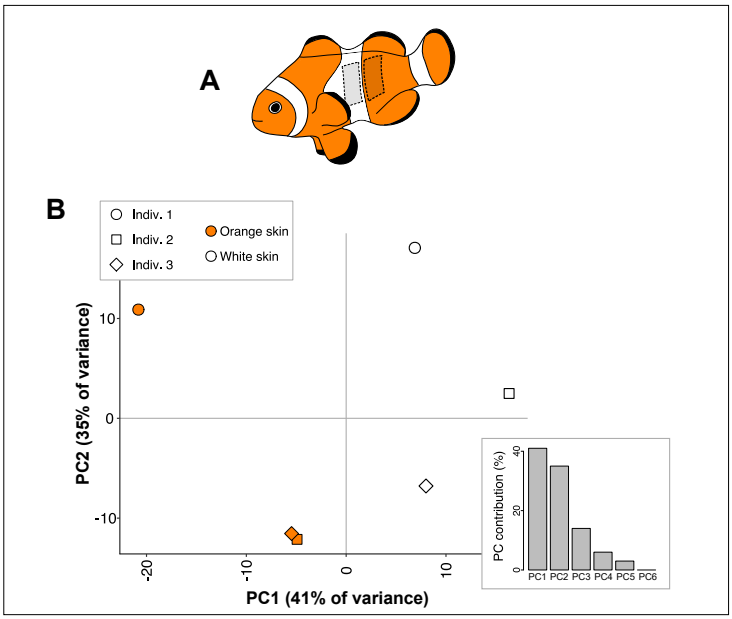

Supplementary Figure 4

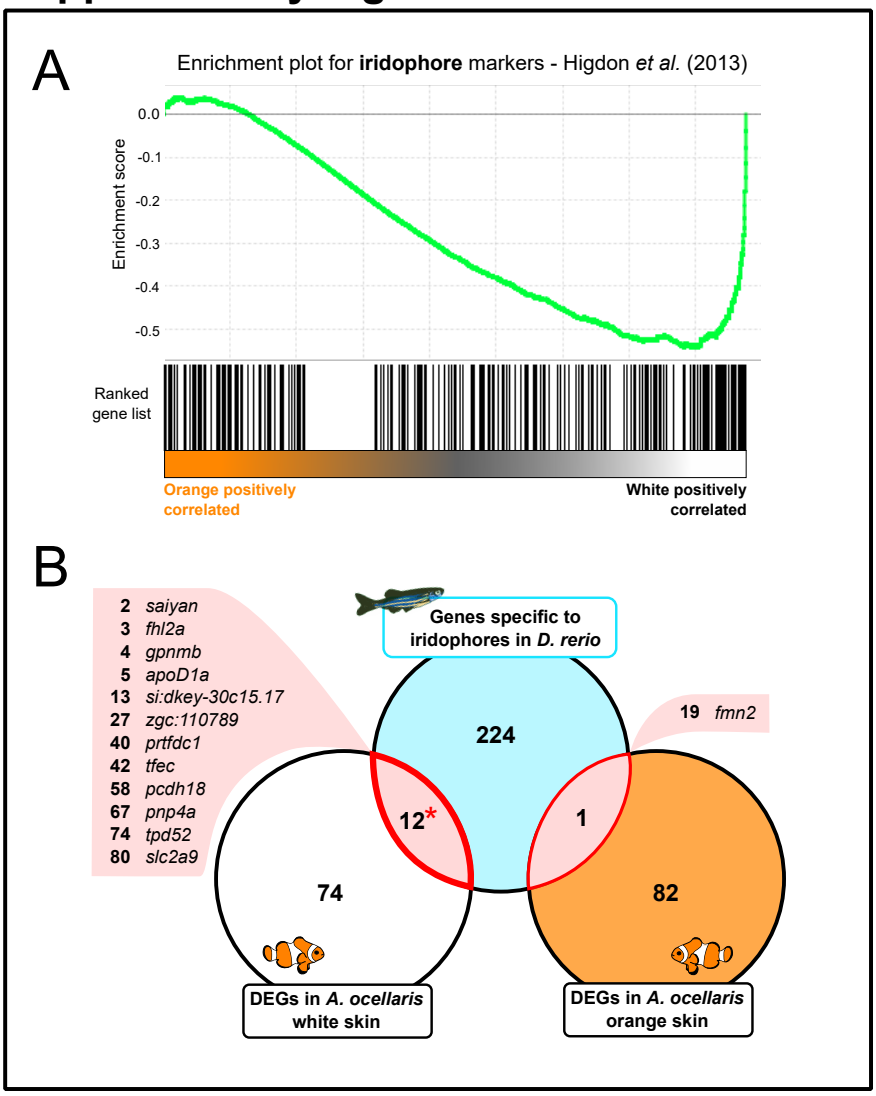

Supplementary Figure 5

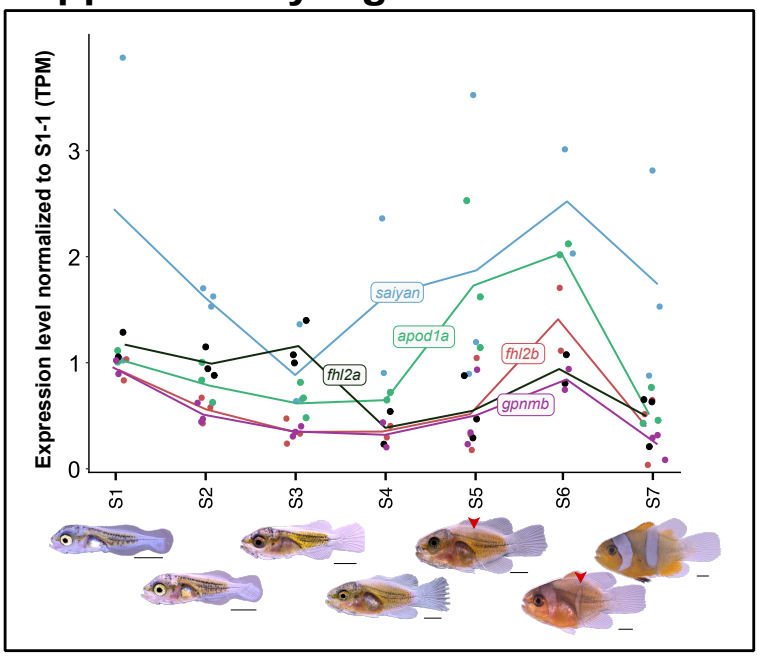

Supplementary Figure 6

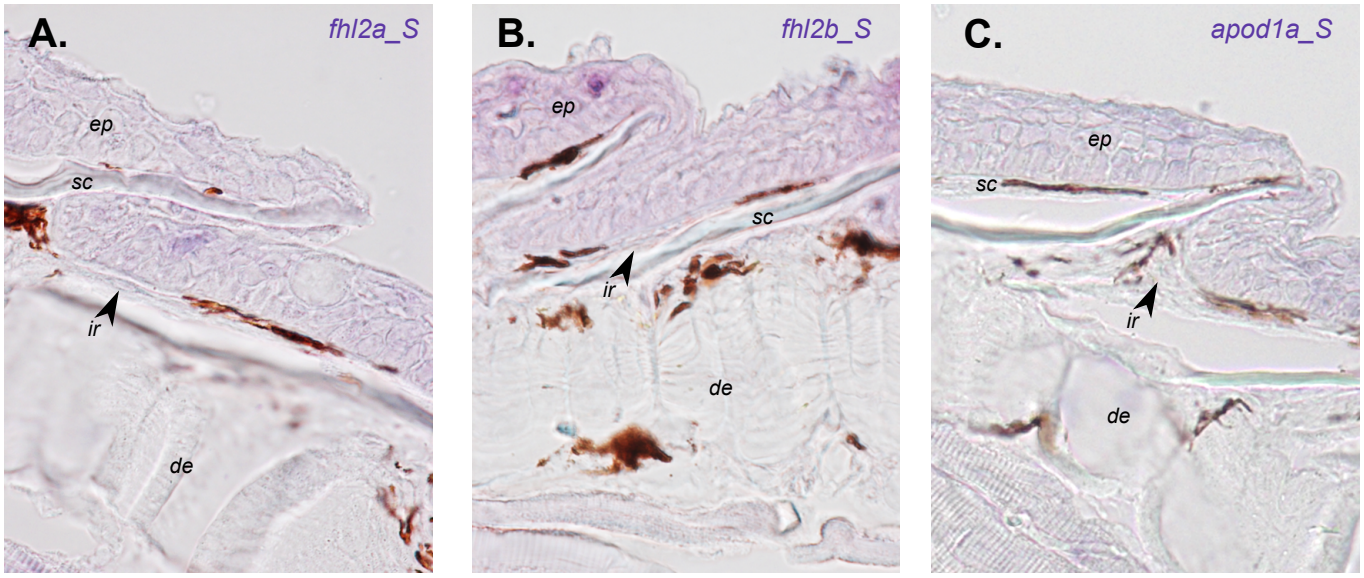

Supplementary Figure 7